Tests of a high density polarized ^{3}He target for electron scattering

T. E. Chupp and R. A. Loveman*
Harvard University Physics Laboratories, Cambridge, Massachusetts 02138

A. K. Thompson, A. M. Bernstein, and D. R. Tieger
Physics Department, Laboratory for Nuclear Science, and Bates Linear Accelerator Center, Massachusetts Institute of Technology, Cambridge, Massachusetts 02139
(Received 5 August 1991)

We have developed a polarized ^{3}He target for polarized electron scattering measurements. The target has a ^{3}He density of 1.1×10^{20} nuclei cm^{-3}, a total length of 7.5 cm and thin glass windows of 120–180 μm thickness. ^{3}He polarization as large as 40% was produced, limited only by the available laser power. The ^{3}He polarization was maintained during bombardment with up to 22 μA of 578 MeV electrons. A measurement of elastic scattering of polarized electrons from polarized ^{3}He confirmed that the nuclei in the electron beam had the expected polarization. The polarization is produced by spin exchange with laser optically pumped Rb vapor, and the target design incorporates two separated volumes, one for optical pumping and the other for the electron bombardment. Extensions of this design are practical for fixed target electron scattering from polarized ^{3}He planned for SLAC and CEBAF.

PACS number(s): 24.70.+s, 25.30.Bf, 29.25.Pj

I. INTRODUCTION

High density polarized ^{3}He targets using spin exchange with laser optically pumped Rb vapor [1] have recently been utilized as a neutron polarizer for epithermal neutrons at LAMPF [2] and as a target at TRIUMF for several measurements with beams of up to 100 nA of polarized and unpolarized protons [3,4]. Studies of polarized muon capture on polarized ^{3}He are also underway at LAMPF [5]. Because the high density target can provide target areal density of $(5-100)\times10^{20}$ ^{3}He/cm^3 it is also appropriate for a number of measurements that have been proposed for scattering of polarized electrons from a fixed target of polarized ^{3}He with the particular motivation of extracting the neutron's elastic form factors [6,7] and spin-dependent deep inelastic structure functions [8,9]. These electron scattering experiments require beam currents of 10–50 μA which leads to several technical requirements not faced by the targets described in references [1–5]. Understanding of these requirements will follow from the discussion of the principles of Rb optical pumping and ^{3}He polarization; however, they are enumerated in this introduction. They are the following: (i) The electron beam must penetrate windows that survive the heat load and radiation field as well as maintain a surface suitable for containing the polarized ^{3}He; (ii) the effect of the ionization on Rb optical pumping [10] must be eliminated; (iii) "glass blackening," i.e., the formation of color centers within the glass due to the high radiation field of the electron beam, must be accommodated; and (iv) the relaxation rate of ^{3}He polarization due to ionization along the electron beam must be negligible relative to the replenishment rate of polarized ^{3}He.

These requirements have been successfully incorporated into a two chamber target (see Fig. 1) which separates the volume in which the Rb optical pumping and ^{3}He polarization take place and the volume in which electron bombardment occurs. The two volumes are maintained at different temperatures so that the Rb vapor is confined to the pumping cell. A transfer tube of length L and cross-sectional area S connects the two cells. The transfer tube dimensions are chosen so that the time constant for transfer of ^{3}He polarization is much less than any ^{3}He polarization time constant (i.e., for production of ^{3}He polarization and relaxation of the polarization). The two chamber target has provided a ^{3}He density of 1.1×10^{20} nuclei cm^{-3} within a total length of 7.5 cm and a polarization of up to 40%. The polarization was maintained during bombardment by a 22 μA, 578 MeV electron beam.

II. PRINCIPLES OF Rb OPTICAL PUMPING AND ^{3}He POLARIZATION

The development of the technique of spin exchange between ^{3}He and laser optically pumped Rb vapor has been developed over the past five years and described in several previous publications [1,11,12]. In these works, we show that the polarization of ^{3}He produced by spin exchange with laser optically pumped Rb builds up from $P_3(t=0)=0$ to

$$P_3(t)=P_{\mathrm{Rb}}\frac{\gamma_{\mathrm{SE}}}{\gamma_{\mathrm{SE}}+\Gamma}(1-e^{-(\gamma_{\mathrm{SE}}+\Gamma)t}), \quad (1)$$

where P_{Rb} is the average electron spin polarization of the Rb vapor, γ_{SE} is the rate of spin exchange, and Γ is the

*Current address: SAIC, Santa Clara, CA 95054.

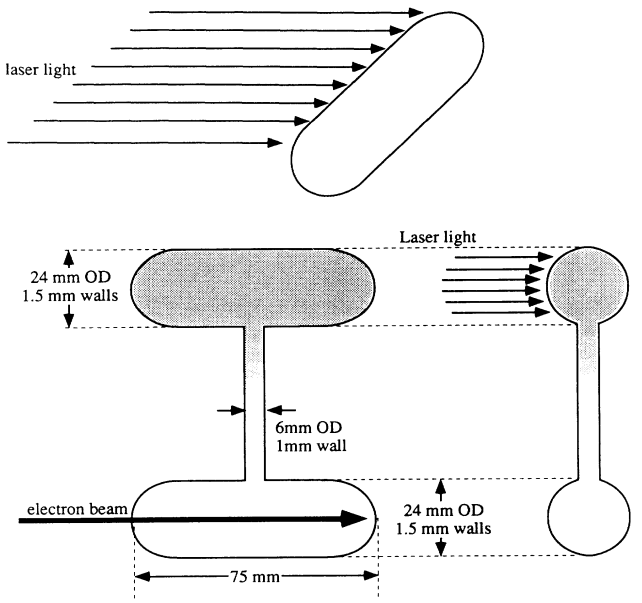

FIG. 1. A schematic illustration of the two-cell target. The upper cell is the pumping volume (V_p) and the lower cell is the target volume (V_t). The Rb is confined to the upper cell by a thermal gradient along the transfer tube.

total relaxation rate for the ^{3}He spin. We also note that when $P_{\mathrm{Rb}}=0$, the relaxation of ^{3}He polarization, originally $P_3(0)$ is given by

$$P_3(t)=P_3(0)e^{-(\gamma_{\mathrm{SE}}+\Gamma)t} . \tag{2}$$

The application of these equations to the two chamber target is straightforward as long as the time constant for polarization transfer from the pumping cell to the target cell is much less than the time constants for ^{3}He polarization and relaxation. The validity of this assumption is demonstrated by the measurement of transfer times described in Sec. V. We find a polarization transfer time of 10 min compared with polarization and relaxation times of several hours to tens of hours. The two chamber target can then be considered as a single total volume equal to the sum of a pumping cell volume (V_p) and target cell volume (V_t) with the Rb confined to the pumping cell (see Fig. 1).

In the pumping cell, spin exchange mediated by the effective hyperfine interaction occurs between the polarized Rb valence electron and the ^{3}He nucleus. The hyperfine interaction is relatively weak ($\omega_{\mathrm{HF}}\approx 100$ MHz) and the collision duration is short ($\approx 10^{-12}$ s) so that the probability of spin exchange during a single collision is small and many collisions are required. Expressed in terms of a velocity-averaged rate constant [13,14]

$$k_{\mathrm{SE}}=\langle \sigma_{\mathrm{SE}} v \rangle = 1.2\times 10^{-19}\ \mathrm{cm}^3\ \mathrm{s}^{-1} , \tag{3}$$

the polarization rate per ^{3}He is

$$\gamma_{\mathrm{SE}}=n_{\mathrm{Rb}}k_{\mathrm{SE}}\frac{n_pV_p}{n_pV_p+n_tV_t} , \tag{4}$$

where n_{Rb} is the Rb vapor density in the pumping cell and n_p and n_t are the ^{3}He number densities in the two cells which are in general not equal due to the temperature difference of the pumping cell and target cell. Thus

$$n_{\mathrm{Rb}}\frac{n_pV_p}{n_pV_p+n_tV_t} \tag{5}$$

is the average Rb number density encountered by each ^{3}He atom throughout the two cells. In our target, n_{Rb} varies from 4×10^{14} to 6×10^{14} atoms cm^{-3} and γ_{SE} varies from $1/(12\ \mathrm{h})$ to $1/(8\ \mathrm{h})$.

^{3}He relaxation rates are discussed in detail in Sec. III. Contributions are wall relaxation, magnetic-field effects and ionization induced relaxation. In general, the ^{3}He relaxation rates will be different in the pumping cell and the target cell since the contribution of ionization should affect only the target cell and since contributions due to the magnetic fields produced by the electron beam will also be greatest in the target cell. We will therefore write the average relaxation time for the two cell target in terms of contributions in the individual cells:

$$\Gamma=\Gamma_p\frac{n_pV_p}{n_pV_p+n_tV_t}+\Gamma_t\frac{n_tV_t}{n_pV_p+n_tV_t} , \tag{6}$$

where Γ_p and Γ_t are actually averages of the relaxation rates throughout each cell.

With the assumption that the transfer time is much less than the other time constants, the equilibrium ^{3}He polarization in the two chamber target can be expressed as follows:

$$P_3(t\rightarrow\infty)=P_{\mathrm{Rb}}\frac{n_{\mathrm{Rb}}k_{\mathrm{SE}}n_pV_p}{n_{\mathrm{Rb}}k_{\mathrm{SE}}n_pV_p+\Gamma_pn_pV_p+\Gamma_tn_tV_t} , \tag{7}$$

where P_{Rb} is the average Rb polarization in the pumping cell.

In the Appendix, we derive equations fully describing the dynamics of the two cell target. It is shown there that Eq. (7) follows in the limit that the polarization-transfer time constant is much less than all other time constants. Rb optical pumping is discussed in the following paragraphs and ^{3}He polarization relaxation is discussed in Sec. III.

A. Rb optical pumping

Natural Rb has two isotopes: ^{85}Rb with nuclear spin $\frac{5}{2}$ and abundance 72.17% and ^{87}Rb with nuclear spin $\frac{3}{2}$ and abundance, though radioactive, 27.83%. In practical situations of high ^{3}He and N_2 density, the width of the $5s_{1/2}$-$5p_{1/2}$ ($D1$) resonance is determined by the rate of collisions that destroy coherence between the ground state and excited state. This collisional width is about 18 GHz per amagat (1 amagat $= 2.7\times 10^{19}$ molecules cm^{-3} is the number density of a gas at standard temperature and pressure). The collisional width is much greater than the hyperfine splittings and isotope shift [15]. Therefore broadband laser light of 3–30 GHz bandwidth can be used to optically pump both hyperfine levels of natural Rb [12]. Furthermore, the hyperfine interaction strongly

couples the electron spin and nuclear spin so that the electron polarization varies from $\langle s_z \rangle = -\frac{1}{2}$ to $\langle s_z \rangle = \frac{1}{2}$ as m_F changes from $-f$ to f. In spite of these complications, the optical pumping process can be accurately illustrated by consideration of Fig. 2, in which the nuclear spin is neglected and only the valence electron spin is considered.

When circularly polarized light is tuned to the $D1$ resonance wavelength of 794.7 nm only the $5s_{1/2}$ ground state with magnetic projection labeled $m_s = -\frac{1}{2}$ absorbs the light. Due to the high collision rate with buffer gas atoms of ^{3}He and N_2, the $5p_{1/2}$ states will be mixed and every ground state will be equally repopulated. The population of the $m_s = +\frac{1}{2}$ state therefore increases as the population from the other ground-state sublevel is pumped into it. The Rb vapor becomes electron spin polarized and transparent to the σ_+ photons.

Relaxation of the ground-state polarization or spin destruction is indicated by the rate Γ_{SD}. Spin destruction occurs due to the couplings of the valence electron spins at the container walls and during collisions with other Rb atoms, ^{3}He and N_2. The dominant relaxation mechanisms for Rb polarization in our target are collisions between pairs of polarized Rb atoms [16] and with the ^{3}He and N_2 atoms as well as diffusion to the cell walls [17]. A complete treatment of this problem is provided in a separate publication [17], and we write only the result

$$\Gamma_{SD} = 2\times10^{-18} n_3 + 8\times10^{-13} n_{Rb} + 8\times10^{-18} n_{N_2} , \quad (8)$$

where the n's are the number densities of the respective species. The laser light must provide angular momentum to the target at the rate per Rb atom of Γ_{SD} in order to maintain a steady-state polarization. For our high density ^{3}He target with $n_3 = 1.1\times10^{20}$, $n_{Rb} = 6\times10^{14}$ atoms cm^{-3} and 100 torr of N_2, $\Gamma_{SD} = 710$ s^{-1}.

The relaxation of Rb electron spin due to diffusion to the cell walls results in a boundary layer of unpolarized Rb that absorbs the incident light. This absorption is accounted for by increasing the incident light intensity by approximately $n_{Rb}\sqrt{10.8 D\sigma_{abs}/I}$, where σ is the absorption cross section for the incident light, D is the diffusion constant for Rb in ^{3}He ($D = D_0 n_0/n$, and $D_0 = 0.3$ cm^2/s and $n_0 = 1$ amagat), and I is the intensity of incident photons (rate per unit area). The factor of 10.8 accounts for the wall collision loss of the total angular momentum ($\mathbf{F} = \mathbf{S} + \mathbf{K}$) stored in the Rb atoms. For our conditions, this layer absorbs about 15% of the incident laser intensity. This loss might be reduced with appropriate wall coatings such as discussed by Swenson and Anderson [18]. We therefore require at least 3 W of laser power for our 25 cm^3 pumping cell at $n_{Rb} = 6\times10^{14}$ atoms/cm.^{3}

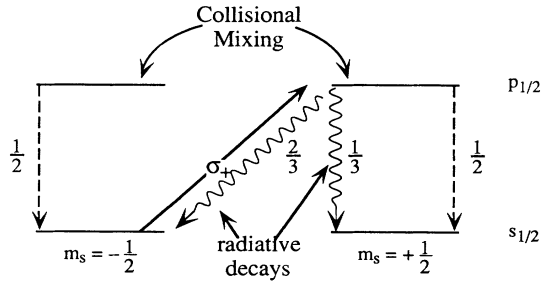

FIG. 2. Illustration of Rb optical pumping for incident circularly polarized (σ_+) light. Only the ground state with $m_s = -\frac{1}{2}$ is depopulated by the σ_+ light. Due to collisions with the ^{3}He and N_2 gas in the pumping cell, the $p_{1/2}$ states are mixed and the probability for repopulating each ground state is $\frac{1}{2}$.

The effect of ionization on Rb polarization is also quite serious, though not well understood. We have observed the effects of beams of about 100 nA of 20 MeV alpha particles [10] and several μA of 250 MeV electrons. The Rb polarization is greatly reduced in a single cell target. This problem has been eliminated in the two cell target design which isolates the polarized Rb vapor from the region of electron bombardment.

Another mechanism that can in principle limit P_{Rb} at high n_{Rb} is radiation trapping due to the emission of unpolarized, resonant photons trapped within the high density Rb vapor. Radiation trapping is suppressed by including N_2, which nonradiatively quenches the Rb excited states [19]. We use about 4×10^{18} molecules cm^{-3} or 100 torr at 300 K of N_2. This N_2 also reduces the effects of ionization on ^{3}He relaxation as discussed in Refs. [10,20]. The possibility of using as little as 20 torr of N_2 or alternatively using H_2 is under investigation.

It is therefore possible to produce essentially 100% polarization of the Rb in the pumping volume, limited only by shadowing which prevents the laser light from reaching some parts of the vapor.

III. ^{3}He POLARIZATION RELAXATION

The total ^{3}He spin relaxation rate Γ of Eq. (1) is the sum of rates due to wall interactions, collisions, magnetic-field inhomogeneity, and the ionization produced along the electron beam. Wall relaxation rates have been observed to vary appreciably depending most strongly on the material used for the cell. Borosilicate glasses such as Pyrex have high helium permeation, and it is believed that the ^{3}He is subject to long effective sticking times as it diffuses into the glass. Glasses with very low helium permeation such as alumino-silicate glasses (Corning 1720 and 1723) and Schott 8290 have much longer wall relaxation times. For Corning 1720, a wall relaxation rate smaller than 1/(60 h) has been observed while for Schott 8290 glass, 1/(30 h) has been observed. Bulk relaxation due to He-He collisions contributes a rate 1/(80 h) for a 10 atmosphere target.

A. ^{3}He polarization relaxation due to magnetic-field gradients

Both static and time-dependent magnetic fields lead to ^{3}He polarization relaxation. In this section we present a general formulation of the problem and derive approximate expressions for relaxation contributions due to both static gradients and the time-dependent fields produced by the electron beams encountered at labs such as Bates and SLAC. Our formulation assumes the limit of high density and high magnetic field appropriate for the high

density targets [21]. We first consider relaxation due to magnetic field gradients. We define an average magnetic

$$\mathbf{B}_0 = B_0\hat{\mathbf{z}} = \frac{1}{V}\int \mathbf{B}(\mathbf{r})d^3r \ . \tag{9}$$

Magnetic-field gradients have components parallel and transverse to $\mathbf{B}_0$. At a specific position $\mathbf{r}$, the transverse components of $\mathbf{B}$ are given by $\mathbf{B}_T(\mathbf{r})$ with

$$\int \mathbf{B}_T(\mathbf{r})d^3r = 0 \ . \tag{10}$$

As a ^{3}He atom moves rapidly (with velocity about 10^5 cm/s) between collisions with other gas molecules $\mathbf{B}_T$ changes and therefore the direction of $\mathbf{B}(\mathbf{r})$ changes. Thus in the atom's rest frame, there is a rotating field. The evolution of an atom's spin is found by integration of the Schrödinger equation during the interval τ_c that begins and ends with a gas kinetic collision. We are interested in the angle of rotation of the spin relative to $\mathbf{B}_0$: θ. The change of polarization during the interval is

$$\Delta P_3 = P_3(\cos\theta - 1) \approx -P_3\frac{\theta^2}{2} \ , \tag{11}$$

where

$$\theta \approx \frac{\Delta B_T}{\Delta B_z + B_0} \ . \tag{12}$$

ΔB_T is the change of the transverse component of the magnetic field and ΔB_z is the change in the longitudinal component during the interval. We have assumed that the changes ΔB_T and ΔB_z are small compared to B_0. The rate of loss of polarization is given by the average over time and the appropriate volume of the product of $\theta^2/2$ and the collision rate per atom. This averaging in general requires solution of the diffusion equation which is presented in the Appendix. There we show that dP_3/dt is essentially constant over the entire volume. Thus with the assumption that $\theta \ll 1$,

$$\frac{dP_3}{dt} = -\Gamma_B P_3 = -P_3\frac{\theta^2}{2}R \ , \tag{13}$$

where R is the rate of depolarizing events, in this case the traversing of the gradient of B_T between a pair of successive gas-kinetic collisions.

For a static-field gradient, R is the gas-kinetic collision rate given by $R = v/\lambda$, where v is the mean speed and λ is the mean free path. The average over all directions gives $(\Delta B_T)^2 = (\lambda^2/3)(\nabla B_T)^2$. Thus the contribution to the polarization relaxation rate given by Eq. (13) is

$$\Gamma_B = \frac{1}{2}D\frac{(\nabla B_T)^2}{B_0^2} \ , \tag{14}$$

where $D = \frac{1}{3}\lambda v$ is the diffusion constant. This agrees with previously derived expressions for relaxation due to static magnetic-field gradients with the conditions of our high density target [13,21]. This contribution to the ^{3}He relaxation rate can be made negligibly small with control of the field gradients through proper magnet design, magnetic shielding, and by increasing B_0.

The relaxation due to the magnetic field produced by the pulsed electron beam depends on the time structure, peak currents, and beam size. Three effects must be considered. These are the following: (i) Possible coincidence of the ^{3}He Larmor frequency with the harmonics of the electron beam pulse frequency. (ii) The sudden periodic appearance of transverse magnetic-field components due to the beam microstructure. (For example, at both SLAC and Bates Linacs, this microstructure consists of pulses of several ps duration at 300 GHz. The electron beam is pulsed with 1.6 and 16 μs duration at 120 and 600 Hz, respectively, for SLAC and Bates.) (iii) The gradients of the magnetic field produced by the beam which have the time structure described above. The solution to the possible coincidence of the ^{3}He Larmor frequency and pulse frequency harmonics lies in detuning and shifting the Larmor frequency such that this effect becomes negligible. (Harmonics of the beam pulse frequency generally decrease in amplitude as the harmonic number increases.)

To determine ΔB_T and ∇B_T, we assume a Gaussian charge density for the beam:

$$j_b(r) = \frac{I}{\pi a^2}e^{-r^2/a^2} \ , \tag{15}$$

where I is the peak current of the electron beam and a is the nominal beam radius, taken to be 0.05 cm. The resulting magnetic field will be azimuthal and is given by

$$B_\phi = \frac{\mu_0 I r}{2\pi a^2}e^{-r^2/a^2} \ , \tag{16}$$

and its gradient is

$$\nabla B_\phi = \frac{\mu_0 I}{2\pi a^2}\left[1 - 2\frac{r^2}{a^2}\right]e^{-r^2/a^2} \ . \tag{17}$$

To calculate the effects of gradients of the beam during a pulse, the rate R of Eq. (13) must be replaced by $F_D v/\lambda$, where F_D is the duty cycle of the beam, essentially the probability that the ^{3}He atom will undergo a collision while the perturbing field ΔB is present. With $(\Delta B_T)^2 = (\lambda^2/3)(\nabla B_\phi)^2$, the contribution to the relaxation rate, when averaged over the cell of radius A, is

$$\begin{aligned}\Gamma_B &= DF_D\left[\frac{\mu_0 I}{4\pi a A B_0}\right]^2\left[1 - e^{-2A^2/a^2}\left[1 + 4\frac{A^4}{a^4}\right]\right] \\ &\approx DF_D\left[\frac{\mu_0 I}{4\pi a A B_0}\right]^2 \ ,\end{aligned} \tag{18}$$

where the approximation is valid for the values $a = 0.05$ cm and $A = 1$ cm.

The contribution to relaxation from the beam pulse structure is given by considering the sudden appearance of transverse components of the magnetic field which lead to the precession of the ^{3}He spins about $B_{\text{total}} = \mathbf{B}_0 + \mathbf{B}_T$. We can then use Eq. (13) with ΔB_T the transverse component of the instantaneous magnetic field and R the pulse rate. Thus Γ_B averaged over the target cell becomes

TABLE I. Contributions to Γ.

Lab	R	F_D	I	Γ_B^{-1} gradients	Γ_B^{-1} pulsed beam	Γ_i^{-1}
Bates	600 s^{-1}	1×10^{-2}	1 mA	3×10^6 h	40000 h	36 h
SLAC	120 s^{-1}	2×10^{-4}	25 mA	8×10^5 h	340 h	72 h
CEBAF		1	25 μA	6×10^8 h		14.4 h

$$\Gamma_B=\frac{R}{2}\left[\frac{\mu_0 I}{4\pi AB_0}\right]^2\left[1-e^{-2A^2/a^2}\left[1+2\frac{A^2}{a^2}\right]\right]$$
$$\approx\frac{R}{2}\left[\frac{\mu_0 I}{4\pi AB_0}\right]^2 . \quad (19)$$

Estimates of these relaxation rates are presented in Table I.

B. ^{3}He relaxation due to ionization

Ionization of the ^{3}He by the electron beam causes relaxation due to the coupling of the nuclear spin to unpaired electron spins and the rotational angular momentum of He_2^+ molecular ions [20]. When a ^{3}He atom is ionized, the hydrogenlike $^3He^+$ ion with nuclear spin polarization ($m_K=+\frac{1}{2}$) has a probability of 50% electron spin $m_s=+\frac{1}{2}$ and 50% probability of electron spin $m_s=-\frac{1}{2}$. For the case of $m_s=-\frac{1}{2}$, $m_F=0$ and the hyperfine interaction mixes nuclear and electron spin, resulting in some nuclear depolarization. When $m_s=+\frac{1}{2}$, no depolarization occurs. If the ion's lifetime is long enough (more than a few ns), the hyperfine interaction completely mixes the electron and nuclear spins in the $m_F=0$ state and the probability of nuclear depolarization of that ion is $\frac{1}{2}$. This will also lead to some polarization of the electron. If the depolarized ion undergoes charge exchange with other polarized ^{3}He atoms, further nuclear depolarization occurs, but each charge exchange increases the polarization of the ion's electron. When the electron's polarization saturates, it can no longer cause nuclear depolarization. Thus for each electron-ion pair formed, no more than one nuclear spin is depolarized. We characterize this by the quantity n_a, the probability that creation of a single ion pair leads to depolarization of a single ^{3}He nucleus, with $0\le n_a\le 1$.

The exact value of n_a depends on the lifetime of the ion before recombination (τ_a), the mean time between resonant charge exchange collisions which transfer the partially polarized electron between ^{3}He atoms (τ_{ex}) and the rate of hyperfine mixing, estimated to be $A/\hbar=2\pi\times2.6$ GHz [20]. In the limit $A\tau_{ex}/\hbar\ll1$ only a very small amount of polarization is transfered from the nucleus to the electron before a charge exchange collision occurs, and we can estimate n_a using Eq. (13) where

$$\theta=\frac{A\tau_{ex}}{\hbar} . \quad (20)$$

We therefore have for $n_a\ll1$

$$n_a\approx\frac{1}{2}\frac{\tau_a}{\tau_{ex}}\left[\frac{A\tau_{ex}}{\hbar}\right]^2 . \quad (21)$$

In the limit $A\tau_{ex}/\hbar\gg1$ and $A\tau_a/\hbar\gg1$, Bonin *et al.* [20] provide the approximate expression:

$$n_a=\frac{\tau_{ex}+\tau_a}{(2\tau_{ex}+\tau_a)} . \quad (22)$$

In the targets produced for electron scattering with 100 torr of N_2, we have $0.1\le\tau_a\le0.2$ns and $0.01\le\tau_{ex}\le0.03$ ns. Thus

$$0.16<\frac{A\tau_{ex}}{\hbar}<0.5 \text{ rad} . \quad (23)$$

Thus the hyperfine mixing is not complete; however, many charge exchange collisions occur during an ion's lifetime since $\tau_a\gg\tau_{ex}$, and $n_a\approx1$.

The possibility that molecular ions ($^3He_2^+$) form and depolarize ^{3}He nuclei by resonant atom exchange has also been discussed by other authors [1,20,22]. In pure He targets (with no N_2 or other impurity) a single ion can lead to many nuclear depolarizations denoted by n_m, which can be many thousands [22]. Therefore, a fraction $n_{ion}=n_a+n_m$ of the ^{3}He ions formed will depolarize a nuclear spin. In the high density ^{3}He target, $n_{ion}\approx n_a\approx1$ because $^3He_2^+$ formation is so strongly suppressed by the presence of N_2.

The rate of production of $^3He^+$ ions per unit area is

$$R_i=\frac{dE}{d(n_3x)}\frac{n_3 t}{E_i}\frac{j_b}{e} , \quad (24)$$

where $dE/d(n_3x)$ is the energy loss per ^{3}He atom per cm^2, $E_i=32.5$ eV is the energy cost per $^3He^+$-e^- pair, n_3 is the ^{3}He number density, t is the length of the target along the beam, and j_b is the current density of the electron beam given by Eq. (15).

The rate at which ^{3}He atoms relax per unit area is related to R_i as follows:

$$n_3 t\Gamma_i(r)=n_{ion}R_i(r) . \quad (25)$$

Equation (25) can be used to determine the distribution of polarization in the target cell. In the Appendix, we do this and show that the rate of diffusion of ^{3}He atoms into and out of the region of the electron beam is much greater than the relaxation rate of ^{3}He polarization in any part of the target cell. Therefore we can integrate Eq. (25) over the entire volume to determine an average ionization-induced relaxation rate:

$$\Gamma_i=k_{ion}\frac{t}{V_t}i_b , \quad (26)$$

where $i_b = \int j_b d\sigma = j_b(\pi a^2)$ is the total beam current (in ampere) and

$$k_{\text{ion}} = n_{\text{ion}} \frac{dE}{d(n_3 x)} \frac{1}{E_i} \frac{1}{e} . \quad (27)$$

For the high density target, $k_{\text{ion}} \approx 2.4$ cm^2/C and for a 10 μA electron beam and a 1 cm radius target cell, $\Gamma_i = 1/(36\text{ h})$.

In Table I, we estimate the maximum contributions to ^{3}He relaxation due to the effects of the electron beam for Bates, SLAC, and CEBAF. For Bates, we use a beam current of 10 μA and for SLAC, a beam current of 5 μA and a target density three times that used for the Bates estimates. For CEBAF the higher density and a 25 μA continuous beam are assumed. This is less than the projected available beam current for CEBAF and is chosen so that Γ_i is not unreasonably large. In each case, we assume a beam diameter of 1 mm that the static field gradients are minimized, that there is no coincidence of the pulse frequency harmonics with the Larmor frequency, and that $B_0 = 30$ G.

IV. POLARIZED ^{3}He TARGET CONSTRUCTION

The general layout of the polarized target is shown in Fig. 3. The major components are the target cell itself, the laser, heating and cooling stages for the pumping and target cells, and the magnetic field and NMR coils. Specifics of these elements are described in this section.

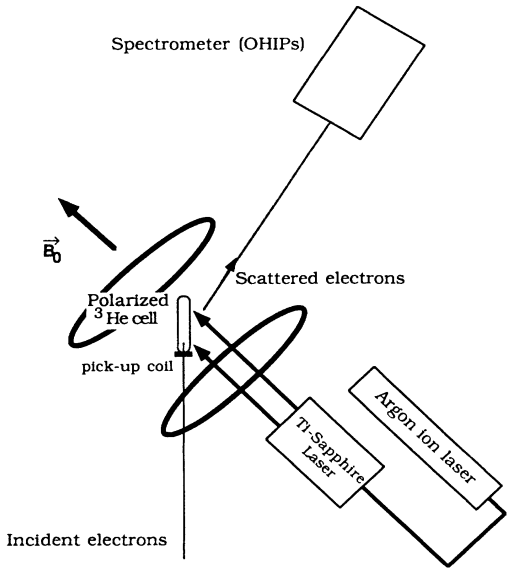

FIG. 3. General layout of the polarized target. The laser light—3 to 4 W at 795 nm—is produced by a Ti:sapphire laser pumped by a 20 W argon-ion laser. The circularly polarized light is incident along the main static magnetic field ($\mathbf{B}_0$) onto the pumping cell.

A. Target cells

The target cell design is illustrated in Fig. 1. The target is constructed entirely of glass in order to provide sufficiently long wall relaxation times for ^{3}He polarization ($\Gamma_w^{-1} > 15$ h). We have used two kinds of aluminosilicate glass—Corning 1720 and Schott 8290. For the two cell targets similar wall relaxation times have been observed for the two kinds of glass, varying from 2 to 30 h. The source of the inconsistency of these relaxation times remains unknown but may arise in the glass fabrication or glass blowing stage or due to impurities in gases used to fill the cells [23,24].

The glass stock used consisted of standard tubing. For the Schott 8290, the pumping cell and target cells are made from 2.2 cm inside diameter, 0.07 cm wall thickness tubing. The cells are cylinders of length 6.5 to 7.5 cm with rounded ends. For the pumping cell, standard thickness seals are used to close the ends of the cells. For the target cell, thin-end windows are blown by spinning the cell to thin the glass, and then the ends are thinned further by blowing them out. The window thickness was determined by measuring x-ray attenuation. Window thicknesses varied from 120 to 180 μm. A single transfer tube connects the two cells. The transfer tube is 5 cm long and made from 0.4 cm inside-diameter tubing chosen so that the transfer rate for polarization is about $1/(10\text{ min})$. The measurement of this transfer rate is described in Sec. V. The entire assembly is annealed after the thin windows are blown according to the manufacturer's annealing schedule.

To fill the target with the gases it is connected via the pumping cell to a glass manifold. A side-arm with natural Rb metal in a glass ampoule is attached to the manifold, and the manifold is connected to an all metal vacuum system through a Viton O-ring compression seal. The vacuum system employs an ion pump and sorption pump to maintain cleanliness; however, a liquid-nitrogen–trapped mechanical pump is used to remove helium from the system after a cell is filled.

A target is baked for several days at 400 °C to drive volatile material from the glass surface. Additional cleaning with an rf discharge is employed. The base vacuum after baking, measured at the ion pump, is less than 10^{-7} torr.

The Rb is distilled and introduced into the pumping cell by chasing it along the glass tube of the manifold with a torch. During this procedure, the high vacuum pumping continues so that any material out gassed by the Rb and the glass surfaces is pumped away. This procedure is never exactly reproducible and may contribute to the observed variation of ^{3}He wall relaxation rates. A visible amount of Rb metal is introduced into the pumping cell, which forms a shiny coating on part of the glass surface. We estimate that several milligrams of Rb are present.

The N_2 gas is then introduced into the manifold. The N_2 pressure of 100 torr at room temperature (300 K) is measured with a capacitance manometer. The target is then valved off from the manifold and the entire target is immersed in liquid nitrogen at 77 K. The N_2 is pumped

out of the manifold and ^{3}He is introduced at a pressure of about 2600 torr. When the valve to the target is opened, the ^{3}He fills the target that is at a temperature of 77 K and a pressure of about 720 torr as measured with the capacitance manometer. The cell is then sealed with a torch by melting the glass just above the target which collapses due to the greater outside pressure of the atmosphere, thus forming a fused seal. While the seal is made, the entire target remains at liquid-nitrogen temperature and the pressure is monitored. The final densities of ^{3}He and N_2 in the target are determined from the pressure and temperatures at the time of sealing and the N_2 pressure before sealing. Measurement of elastic scattering described below confirm these densities. Cleanliness of the N_2 and ^{3}He gases has been shown to be crucial for optimum performance. This has been achieved with liquid-helium cryogenic techniques as reported by Cates *et al.* [23] and Häusser *et al.* [24].

During operation, the target is contained in an assembly consisting of the oven for heating the pumping cell to a temperature of 180 °C with integrated NMR coils. The oven is made of Nylatron-GS, a high temperature plastic, with Pyrex glass windows for the incident laser light and to monitor light transmission and the fluorescence from the Rb vapor. The oven must be constructed of nonconducting plastic instead of a nonmagnetic metal such as aluminum alloy because of the NMR rf fields.

B. Polarization measurement

The ^{3}He polarization is measured using adiabatic fast passage NMR which has been discussed in detail in previous publications [1,14,25]. The coil arrangement consists of three orthogonal axes for $\mathbf{B}_0$, a set of rf drive coils and a pickup coil. The circuitry is illustrated in Fig. 4.

During a polarization measurement, the rf produces an oscillating magnetic field of typical frequency 100 kHz which is tuned far above the Larmor frequency of the ^{3}He. The static field $\mathbf{B}_0$ is then increased at a rate of about 1 G/s until the Larmor frequency greatly exceeds the rf frequency. (In this case far above and far below mean many times the rf linewidth.) In the process, the Larmor frequency sweeps through resonance with the rf frequency and the ^{3}He spin rotates in the laboratory by an angle approaching 180° as long as the process is adiabatic. During the rotation, the spin also precesses at the Larmor frequency and the magnetization of the ^{3}He can be determined by measuring the voltage induced in a pickup coil. The pickup coil forms part of a tuned circuit which is resonant near or above the rf frequency. A measurement of the polarization consists of sweeping B_0 up and down, thus producing a pair of polarization reversals and returning the polarization to its original orientation.

The pickup coil is oriented perpendicular to the drive coil, but it is not possible to completely eliminate the coupling of the drive field into the pickup coil. We therefore employ a diffential measurement using the lock-in amplifier to extract the difference between the pickup coil signal and the rf drive signal shifted in amplitude and phase.

Pickup coils can be attached to monitor the polarization in either the pumping cell or the target cell. For the target cell, a coil can be wound directly around the cell for the geometry shown in Fig. 4. This greatly increases the coupling of the flux and reduces end effects compared to the pumping cell for which the pickup coil must be mounted away from the cell in order not to shadow the laser light.

The NMR system is calibrated by comparison with signals from protons in water that are polarized due to the Boltzman distribution of populations in a magnetic field at thermal equilibrium. The proton polarization (P_1) is quite small:

$$P_1 = \frac{\hbar\omega_{\rm rf}}{2kT} \approx 10^{-8} , \tag{28}$$

but the density of protons in water (6.7×10^{22} ^{1}H/cm^3)

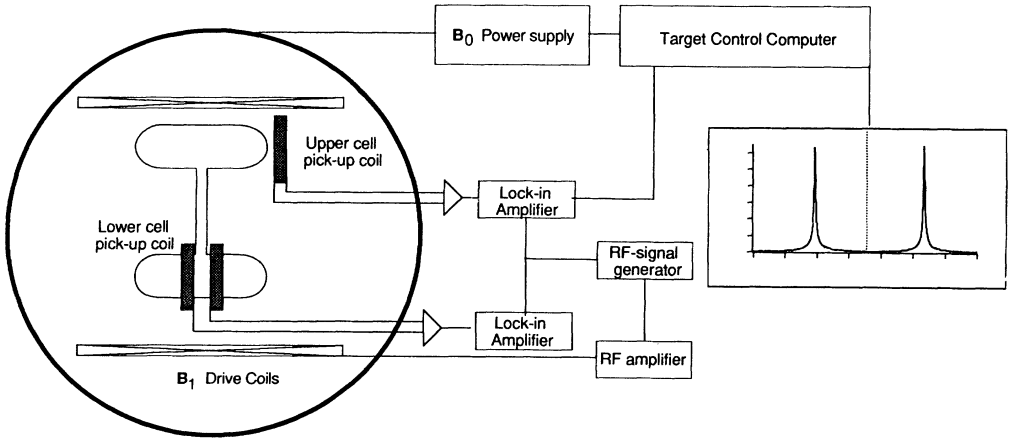

FIG. 4. Schematic of the NMR ^{3}He polarimeter. Pickup coils can monitor the polarization in both the pumping cell and target cell, though during electron bombardment, only the pumping cell polarization is monitored. The control computer sweeps the $\mathbf{B}_0$ field through the resonance of the ^{3}He with the applied rf $\mathbf{B}_1$ field. The magnetization precessing about $\mathbf{B}_0$ at the Larmor frequency induces a voltage in the pickup coil which is detected by the lock-in amplifiers. The computer records the NMR signal vs $\mathbf{B}_0$.

provides sufficient enhancement to measure the signal size with precision of about 5%. Figure 5 shows sample NMR resonance signals from the protons in water. The proton polarization relaxation time is only a few seconds and therefore the polarization, once flipped, relaxes back to that of thermal equilibrium before the return sweep. Since the lock-in response is proportional to the sign of the polarization and the rate of change of B_0, the resonance peaks change sign between the upward and downward sweeps. For the ^{3}He NMR, shown in Fig. 6, both the sign of the polarization and the rate of change of B_0 reverse and the two resonance peaks have the same sense.

The calibration is performed with the same NMR frequency as the ^{3}He in order that the response of the tuned pickup coils not change. It is crucial that the water cell be the same shape and size as the polarized ^{3}He target in order that all of the flux coupled from the complicated geometry be the same for the two.

The ^{3}He polarization is determined from the NMR signal size (S_3) by taking the ratio with the proton signal size (S_1):

$$P_3 = P_1 \frac{S_3}{S_1} \frac{n_1}{n_3} \frac{\mu_1}{\mu_3} , \tag{29}$$

where μ_1 and μ_3 are the magnetic moments of the proton and ^{3}He, respectively. The dominant uncertainties for the quantities used in Eq. (29) are S_1 and n_3. Though the pressure of the target at the time it is sealed is precisely measured with the capacitance manometer, the effects of thermal gradients during sealing with the torch are uncertain. Measuring the remaining pressure in the manifold gives a more accurate measure of the amount of gas in the sealed cell. Operation with a temperature difference between the pumping cell and target cell requires a correction for the temperature. We have independently measured the ^{3}He density in the target cell by elastic scattering of electrons to confirm this. We consider the uncertainty of ^{3}He density to be less than 5%. For the sealed targets, our estimated precision for the ^{3}He polarization measurement is therefore taken to be

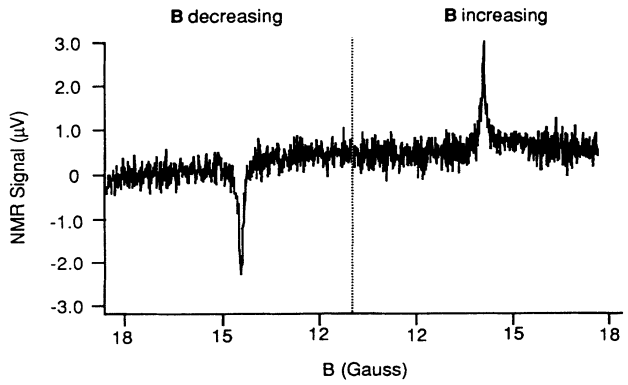

FIG. 5. NMR signals from protons as the $\mathbf{B}_0$ field is swept through the resonance. The sign change of the NMR signals for $\mathbf{B}_0$ decreasing and $\mathbf{B}_0$ increasing is due to the relaxation of the proton polarization to its thermal equilibrium value between sweeps. This is further explained in the text. Signals are from the lower cell pickup coil.

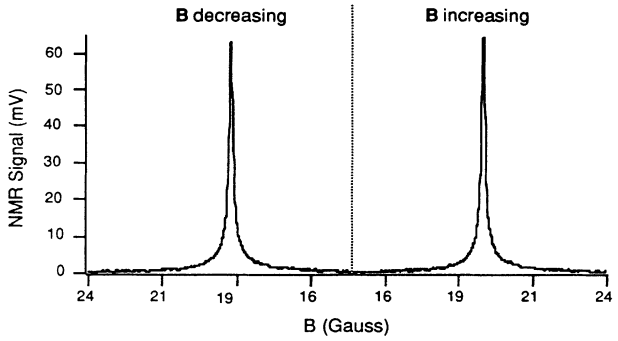

FIG. 6. ^{3}He NMR signals. The ^{3}He polarization does not change appreciably between sweeps and therefore the NMR signals for $\mathbf{B}_0$ decreasing and $\mathbf{B}_0$ increasing have the same sign. Signals are from the upper cell pickup coil.

7%. We have also developed an unsealed target in which the pressure and temperatures are directly measured (see Sec. IX).

C. Lasers

Throughout the course of development of the spin-exchange technique of ^{3}He polarization, dye lasers [1], diode laser arrays [12], and most recently Ti:Al_2O_3 lasers have been used. Under normal operating conditions, Ti:Al_2O_3 lasers are currently capable of producing 5 W of useful power for 20 W of input power from all blue and green lines of an argon-ion laser. Cooling of the crystal to about 10 °C is essential and improves higher power performance. Efficiency of 25% above a threshold of 2 W seems a reasonable expectation.

V. POLARIZATION TRANSFER TIME MEASUREMENT

The performance of the two-cell target has been investigated on the bench and under actual running conditions with an electron beam. In this section we describe the bench-test measurements of the time constants for polarization build up and transfer between the pumping cell and target cell.

The intrinsic cell relaxation times and maximum polarization were measured by a series of NMR scans of the target cell polarization at 20 to 30 min intervals beginning (at $t=0$) with zero ^{3}He polarization. Such a measurement is shown in Fig. 7. The characteristic time constant of 6 h is apparent in these data, as well as the effect of tuning the laser. This is indicated by the annotations of Fig. 7. The maximum polarization achieved, about 40% is limited by laser power, which limits P_{Rb} for a given γ_{SE} and by the intrinsic cell relaxation rate Γ which limits the maximum ^{3}He polarization as given by Eq. (7).

The polarization transfer time was measured by destroying the polarization in the target cell and measuring the target cell polarization at 5 min intervals. Under these conditions, an initial difference in polarizations of the pumping cell and target cell given by $P_p(0)-P_t(0)$ will exist. As shown in the Appendix, the time dependence of the target cell polarization is given by

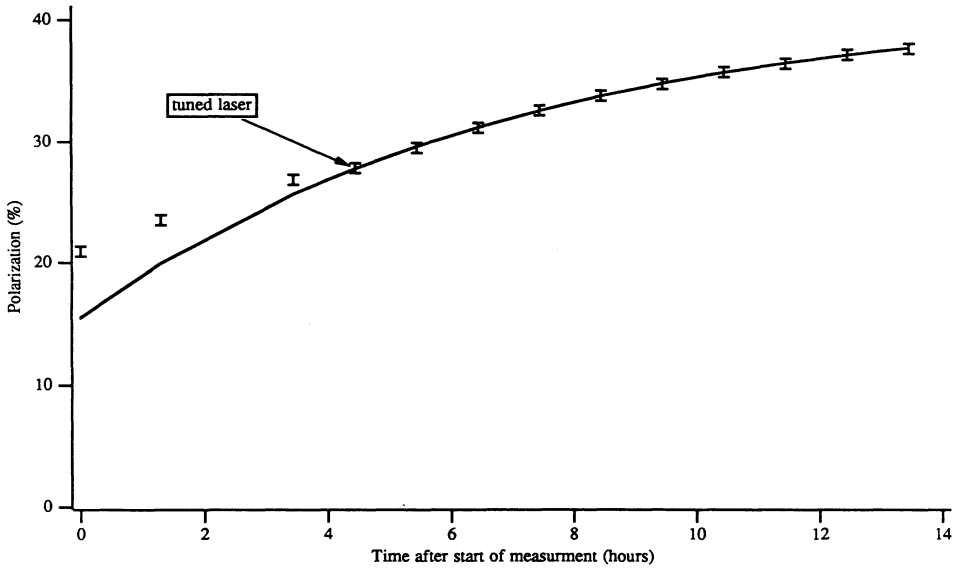

FIG. 7. ^{3}He spin-up curve taken on the bench. During the course of the measurement, the laser was tuned, increasing laser power as indicated. This increased the maximum attainable polarization and indicates that the ^{3}He polarization is laser power limited. The solid curve is a fit to the form of Eq. (1) for the data after the laser was tuned. The time constant for polarization was 6.8 h.

$$P_t(t)=\frac{G_t}{G_p+G_t}[P_p(0)-P_t(0)](1-e^{-(G_p+G_t)t}) , \qquad (30)$$

where P_p and P_t are the ^{3}He polarizations in the pumping and target cells, respectively, and G_p and G_t are rates for polarization transfer into the respective cells. These rates are discussed in detail in the Appendix.

The target cell polarization can be destroyed by effecting a maser pulse when the ^{3}He polarization is oriented with respect to $\mathbf{B}_0$ such that a population inversion exists and the pickup coil resonance coincides with the ^{3}He nuclear magnetic resonance frequency. Alternatively, the strong local gradient from a bar magnet can be used to induce stronger ^{3}He spin relaxation in the target cell than in the pumping cell. Figure 8 shows the buildup of polarization in the target cell after the target cell spin

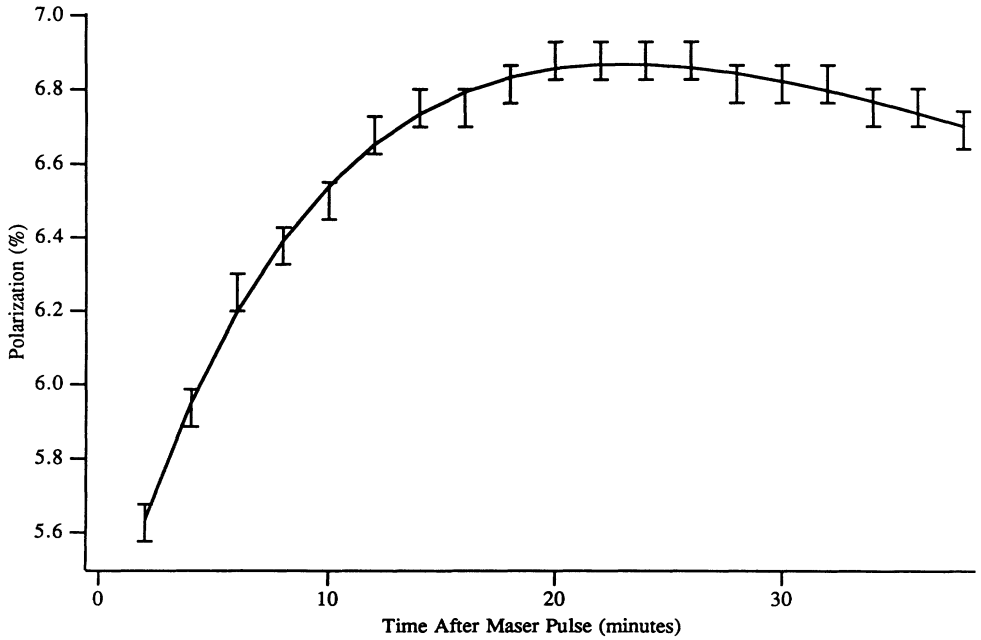

FIG. 8. Measurement of the transfer time for polarization from the pumping cell to the target cell. At the time of the maser pulse, most of the polarization in the target cell was destroyed. The target cell polarization increases as the pumping cell and target cell attain equilibrium. Since the laser was off, the relaxation of spin at the rate Γ_t is apparent. The time constant for polarization transfer is 10 min and the relaxation time for ^{3}He polarization is 5 h, dominated by spin exchange collisions with the unpolarized Rb vapor.

was destroyed. The time constant of 10 min is consistent with the design of the transfer tube and is much shorter than the 6 h time constant for ^{3}He polarization by spin exchange shown in Fig. 7.

The relative size of the time constants for ^{3}He polarization by spin exchange and for polarization transfer from pumping to target cell shows that the two cells are strongly coupled as shown in the Appendix. The ^{3}He polarizations in the pumping and target cells are therefore essentially equal as long as the polarization transfer time is much shorter than any ^{3}He spin relaxation time. This is the case for the work described here, including the in-beam measurements described below. While running with the electron beam, the pickup coils were removed from the target cell and the polarization was measured in the pumping cell only.

VI. IN-BEAM TARGET PERFORMANCE

Several in-beam tests are of interest. First, the effects of the electron beam and radiation on the materials was investigated. The target cells were constructed with 120–150-μm-thick glass windows to reduce the amount of heat produced by incident electron energy loss. These windows have been shown to survive with up to 40 μA of incident current and ran for ten days with 5–7 μA and several hours with 22 μA. Heat was removed by streams of flowing air on both the entrance and exit windows. We have also experienced the effects of the electron beam incident on thicker glass, which melts or weakens the glass as expected. One target cell was destroyed by poor steering of the incident beam into the thicker side wall of the target.

Glass blackening due to the formation of color centers by the high radiation field was also observed. In general, the effects of glass blackening can be reduced by annealing either at high temperature or with ultraviolet radiation. (Sunlight is effective.) Since the pumping cell was maintained at 180–200 °C, it was essentially self-annealing and negligible attenuation of incident laser light due to glass blackening was observed. The target cell was not heated or annealed and significant blackening was observed.

The effect of enhanced ^{3}He relaxation due to ionization was investigated by measuring the polarization time constants. For the 5–7 μA polarized electron beam, we expect a contribution to the ^{3}He relaxation rate of $\Gamma_i = 1/(60\text{ h})$ which is small compared to the combined rates of spin exchange and wall relaxation $[\sigma_{SE} + \Gamma_w \approx 1/(6\text{ h})]$. For a 22 μA unpolarized beam, polarization was maintained for several hours.

In Fig. 9, we show the performance of the target over the course of ten days of running with the 5–7 μA polarized beam. Polarization measurements ae made at approximately 1 h intervals, a time difference short compared to the polarization, and relaxation time constants. Therefore, the polarization during the time between measurements is accurately determined by the average of the measurements at the beginning and end of the interval. Most striking are the long time constants for buildup or decay of polarization and the sudden decrease in the magnitude of ^{3}He polarization associated with certain events such as flipping the polarization, laser failure, etc. Note also that the maximum polarization attained during running was 30%, less than the 40% attained in the bench tests described above. This reduced polarization was due to the different orientation of the pumping cell with respect to the incident laser beam. For the bench test, normal incident was posssible which allowed uniform illumination of almost the entire volume of Rb in the pumping cell. For the in-beam tests, the incident angle was near 45° in order that the ^{3}He polarization be aligned along or perpendicular to the vector q for 578 MeV electrons scattered at 51°. The consequence of the 45° angle degree of incidence for the laser light is that part of the pumping cell was shadowed, and the Rb was not completely illuminated leading to reduced P_{Rb}. An optimal arrangement can be effected with the appropriate choice of orientation of the pumping cell relative to the target cell.

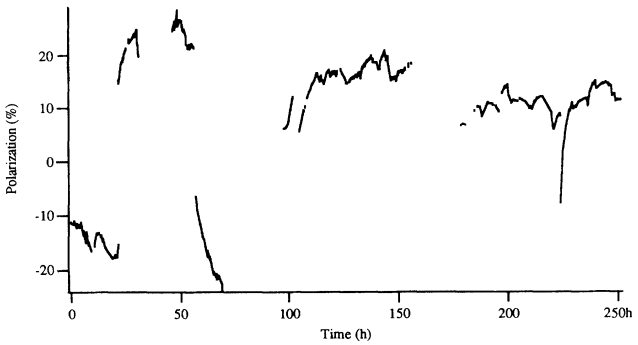

FIG. 9. The polarization during running with the 5–7 μA electron beam. Two different target cells were used.

VII. POLARIZED-ELECTRON-POLARIZED ^{3}He ELASTIC SCATTERING MEASUREMENT

We have used a measurement of elastic polarized electron scattering from our polarized ^{3}He target to confirm the polarization of the ^{3}He in the vicinity of the electron beam. The asymmetries measured in elastic scattering depend only on the previously measured electric and magnetic form factors of ^{3}He [26] and can therefore be accurately predicted without any dependence on models of the nuclear structure of ^{3}He [27]. In a separate paper [28], we describe this measurement in detail. We summarize the results here.

The measurements took place at MIT Bates Linear Accelerator Center where two spectrometers were employed for this measurement. A large solid angle, vertical bend spectrometer with a 10% momentum bite (OHIP's), produced the cleanest data from the extended gas target. A second spectrometer with horizontal momentum analysis and 40% momentum bite (BigBite) was also used to provide additional data, though of lower quality. Target defining slits were used with both spectrometers to screen out electrons scattered from the target end windows. The kinematics are given in Table II. The angles correspond

TABLE II. Energies and angles for elastic scattering asymmetry measurements ($E=0.578$ GeV).

OHIPs $\theta=51.1°$	
E'	0.537 GeV
Q^2	-0.231 (GeV/c)^2
(θ^*,ϕ^*)	(99.8°, 0°)
A_{el} measured	0.43±0.20
A_{el} predicted	0.29±0.015
χ^2	0.49
BigBite $\theta=44°$	
E'	0.546 GeV
Q^2	-0.177 (GeV/c)^2
(θ^*,ϕ^*)	(115.5°,0°)
A_{el} predicted	0.20±0.01
A_{el} measured (D_{avg})	0.13±0.07
χ^2	1.00
A_{el} measured (D_{run})	0.11±0.07
χ^2	1.65
(θ^*,ϕ^*)	(26.4°,0°)
A_{el} predicted	-0.03±0.006
A_{el} measured (D_{avg})	0.19±0.16
χ^2	1.00
A_{el} measured (D_{run})	0.34±0.24
χ^2	1.67

to the scattered electron angle (θ) and the polar angles of the target polarization in a coordinate system with the z axis along the three momentum transfer direction (i.e., along $\mathbf{q}$). $\mathbf{k}$ and $\mathbf{k}'$ are the initial and final electron momenta 0.548 GeV/c is shown in Fig. 10. Peaks for elastic scattering from ^{3}He and ^{14}N as well as inelastic scattering to excited states in ^{14}N are shown. For final electron energy below that corresponding to the ^{14}N elastic peak, inelastic scattering from ^{14}N and ^{3}He produce the broad continuum in the spectrum.

The asymmetry for elastic scattering is extracted by correcting for the electron and target polarization as measured by Møller scattering and NMR, respectively.

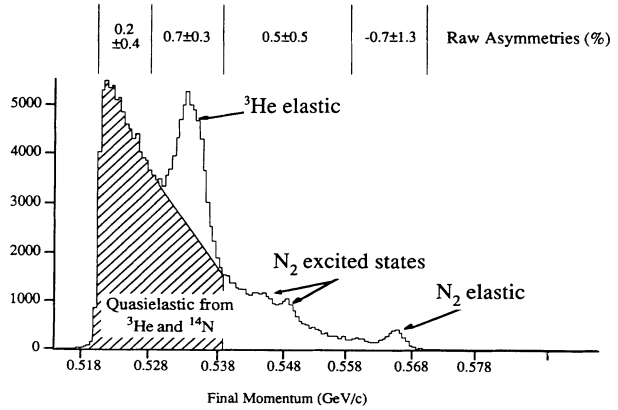

FIG. 10. Spectrum from OHIP's spectrometer. The features due to elastic scattering from ^{14}N and ^{3}He and identified excited states in ^{14}N are indicated. Also indicate are the raw asymmetries, defined in the text, for the regions indicated.

The asymmetry is defined as

$$A_{el}=\frac{1}{P_e}\frac{1}{P_3}\frac{1}{D}\frac{\eta_R-\eta_L}{\eta_R+\eta_L}\ , \tag{31}$$

where P_e is the electron polarization, P_3 is the ^{3}He polarization, D is a dilution factor (the ratio of total counts from ^{3}He to that from all other sources determined from the summed spectrum of all runs with both electron helicities), and $\eta_{R,L}$ are the number of scattered electrons per incident electron for each electron helicity.

For the OHIP's data, we find an asymmetry of $A_{el}=+43\pm20\%$. The errors presented are the combination of statistical and systematic errors. The statistical error dominates all systematic errors including uncertainty of the beam and target polarization. The predicted asymmetry is $+29\pm1.5\%$. For the BigBite data, two different directions of the target polarization are used. The elastic assymmetry for BigBite is extracted by using Eq. (31). Dilution factors were determined in two ways. The first extracts an average dilution factor for all the runs for a given polarization angle by summing the runs D_{avg}, and the second extracts run-by-run dilution factors D_{run} and extracts an asymmetry for each run based on Eq. (31). The results for both techniques are given in Table II for the BigBite data. The two techniques are consistant for the OHIPS data.

We can combine these results by calculating the χ^2 for the measured asymmetries with respect to the predicted asymmetries as given in Table II. The sum for the three measurements is $\chi^2=2.49$ when the BigBite data are analyzed with the averaged data and $\chi^2=3.81$ when the BigBite data are analyzed with dilution factors for each individual run. We therefore conclude that the NMR measurement of polarization and the elastic scattering determination of ^{3}He polarization along the electron beam are consistent. A complete analysis of all of our elastic scattering measurements and further details of the experiment are presented in a separate paper [28].

VIII. FUTURE HIGH DENSITY POLARIZED ^{3}He TARGETS

Several innovations have already been incorporated into single-cell polarized ^{3}He targets at Princeton [23] and TRIUMF [24]. Most important is the production of targets with up to 12 atm of ^{3}He produced by cooling the cell to liquid-He temperatures before sealing. Very long relaxation times, approaching the limit imposed by ^{3}He-^{3}He collisional relaxation [23], have been observed. We plan to use these techniques for two-cell targets as well, which will be essential for the deep inelastic electron scattering work [9]. An alternative technique has been developed which employs a cell that is not permanently sealed, rather having a valve. This has proved useful for our investigations of Rb spin relaxation with various buffer gases [17] and may find an application in an actual target.

Larger target volume seems to be only a question of laser power which is in turn a question of cost. However, in the six years since the first application of laser optical pumping to polarization of ^{3}He by spin exchange, a factor of 5 increase in laser power has been realized with no

increase in cost. Though another factor of 5 may not be realized at a similar, negligible cost, it is likely that the potential for future experiments will be paced by the impressive developments in laser technology, and we hope continued and enhanced cooperation between research and industry.

IX. CONCLUSIONS

We have demonstrated an effective high density polarized ^{3}He target for electron scattering experiments. This was used for a series of tests and masurements at Bates Linac with 5–7 μA of polarized electrons for 10 days and with up to 22 μA of unpolarized electrons for several hours. The two-cell target is necessary for experiments where ionization produced by the incident beam is at a rate that affects Rb optical pumping (greater than about 100 nA for minimum ionizing particles). Measurements of polarization and polarization transfer from pumping cell to target cell demonstrate the principles of operation of the two-cell target. Measurements of asymmetries in elastic scattering of polarized electrons from polarized ^{3}He confirm that the ^{3}He is polarized along the incident beam. The two-cell target design is appropriate for higher volume and density targets for experiments at SLAC and CEBAF which will require significantly greater laser power than used for the work described here.

ACKNOWLEDGMENTS

The authors wish to thank Peter Moulton and Jim Harrison of Schwartz Electro-Optics Inc. for hands on advice on obtaining the optimum high power performance from the Ti::sapphire lasers. We are grateful to M. E. Wagshul and K. von Reden for significant assistance as well as to G. Cates and O. Häusser. We also want to thank G. Dodson, K. Dow, M. Farkhonden, W. Fong, J. Y. Kim, J. M. Richardson, H. Schmieden, T. C. Yates, J. D. Zumbro, G. E. Dodge, and D.J. deAngelis, all of whom took part in data taking at Bates from which the elastic scattering results were extracted. This work was supported by the NSF (Harvard) and DOE under Contract No. DE-AC02-76ER03069 (MIT).

APPENDIX: DYNAMICS OF THE TWO CHAMBER TARGET; TARGET CELL POLARIZATION DISTRIBUTION; TARGET CELL RATE EQUATIONS

In this Appendix, we derive the rate equations describing the dynamics of the two-chamber target, the target cell polarization distribution in the presence of the electron beam, and the target cell rate equations necessary to understand the transfer time measurement. We refer to the Fig. 1 which shows the pumping volume V_p, the target volume V_t, and the transfer tube with length L and cross-sectional area S. In general the temperatures of the two cells are different, which leads to a gradient of ^{3}He density $[n(z)]$ along the transfer tube. The rate equations describe the transfer of spin between the target cell and the pumping cell. In the pumping cell, spin exchange from the laser optically pumped Rb provides a source of spin, and relaxation due to the source described in Sec. III sink the polarization. Additional time dependence is due to the transfer tube connected to the target cell.

1. *Dynamics of the two-chamber target*

We begin by considering a situation in which spin exchange and ^{3}He relaxation are negligible and the only time dependence is due to spin transfer. We consider the density of spin-up and spin-down ^{3}He atoms, n^+ and n^-, respectively. To begin we assume that n^+ and n^- are constants in each of the pumping and target cells but that they are a function of position (z) along the transfer tube. Thus

$$n^+(L/2)=n_p\rho^+(L/2)\ ,\quad n^+(-L/2)=n_t\rho^+(-L/2)\ , \tag{A1}$$

where $\rho^{+/-}$ is the probability of finding a ^{3}He atom with spin up/down, $P_3=\rho^+-\rho^-$ and $\rho^++\rho^-=1$. Also

$$\rho^+(z)=\frac{1+P_3(z)}{2}\quad\text{and}\quad\rho^-(z)=\frac{1-P_3(z)}{2}\ . \tag{A2}$$

A current J^+ of spin-up atoms is driven from the pumping cell toward the target cell by the polarization gradient:

$$J^+(z)=n(z)D(z)\frac{d\rho^+(z)}{dz}=\frac{1}{2}n(z)D(z)\frac{dP_3(z)}{dz}\ , \tag{A3}$$

where $D(z)$ is the diffusion constant for ^{3}He at the temperature and pressure at point z. The rate at which spin up atoms flow from the pumping cell into the transfer tube is related to the rate of change of ^{3}He polarization in the pumping cell given by

$$\frac{dP_p}{dt}=2\frac{d\rho_p^+}{dt}=-\frac{2J_p^+S}{n_pV_p}\ , \tag{A4}$$

and similarly for the target cell,

$$\frac{dP_t}{dt}=2\frac{d\rho_t^+}{dt}=\frac{2J_t^+S}{n_tV_t}\ . \tag{A5}$$

We assume that the polarization gradient is a constant along the transfer tube, and is given by

$$\frac{dP_3(z)}{dz}=\frac{P_3(L/2)-P_3(-L/2)}{L}=\frac{P_p-P_t}{L}\ . \tag{A6}$$

We note that the continuity equation relates the rate of change of polarization along the transfer tube to $J^+(z)$:

$$n(z)\frac{dP_3(z)}{dt}=2n(z)\frac{d\rho^+(z)}{dt}=2\frac{dJ^+(z)}{dz}\ . \tag{A7}$$

With the assumption of Eq. (A6) we find

$$n(z)\frac{dP_3(z)}{dt}=\frac{P_p-P_t}{L}\frac{d}{dz}[n(z)D(z)]\ . \tag{A8}$$

Thus, in the steady state $[dP(z)/dt\rightarrow 0]$, the polarization in the upper and lower cells are equal even when a temperature gradient leads to a finite gradient of $[n(z)D(z)]$. We note also that this assumes that the relaxation of polarization in the transfer tube is negligible. [Such relaxa-

tion can be accounted for by adding a term $-\Gamma P(z)$ to Eq. (A8).

We therefore have

$$J_p^+ = \frac{P_p - P_t}{2L} n_p D_p \quad \text{and} \quad J_t^+ = \frac{P_p - P_t}{2L} n_t D_t \ . \tag{A9}$$

Making use of Eq. (A9), we can define a rate

$$G_p = \frac{D_p S}{L V_p} \ . \tag{A10}$$

Thus the spin transfer rate for the pumping cell is given by

$$\frac{dP_p}{dt} = -G_p(P_p - P_t) \tag{A11}$$

For the target cell,

$$\frac{dP_t}{dt} = -\frac{2J_t^+ S}{n_t V_t} = G_t(P_p - P_t) \ , \tag{A12}$$

where the transfer rate for the target cell is

$$G_t = \frac{D_t S}{L V_t} \ . \tag{A13}$$

In order to include spin exchange and relaxation in the rate equation for polarization in the pumping cell we assume that the Rb is confined to the pumping cell and that sources of ^{3}He polarization in the pumping cell are spin exchange from the Rb and diffusion of spins from the target cell. Relaxation in the pumping cell is due to wall relaxation (Γ_w) and diffusion to the target cell. Thus the time dependence of the polarization in the pumping cell is given by

$$\frac{dP_p}{dt} = -G_p(P_p - P_t) - (n_{\mathrm{Rb}} k_{\mathrm{SE}} + \Gamma_p) P_p + P_{\mathrm{Rb}} n_{\mathrm{Rb}} k_{\mathrm{SE}} \ , \tag{A14}$$

where n_{Rb} is the Rb vapor density in the pumping cell and G_p is the rate of diffusion of polarization into or out of the pumping cell given by Eq. (A10).

2. *Target cell polarization distribution*

For the target cell, electron beam-induced relaxation is position dependent, and we must consider the distribution of the polarization in the target cell. This is determined by solving a rate equation in the presence of the polarization source provided by transfer of spin from the pumping cell, and in the presence of relaxation from all sources: wall relaxation, magnetic fields produced by the electron beam, and ionization. In principle the source of polarization provided by the transfer of spin [Eq. (A12)] is also position dependent, however, the time for diffusion within the target cell is much less than the transfer time. To justify this, we note that the diffusion time from the transfer tube to any part of the target cell a distance d from the transfer tube is given approximately by

$$\tau(d) \approx \frac{d^2}{2D_t} \ . \tag{A15}$$

For $d=4$ cm, appropriate for the targets used in the experiments at Bates, $\tau(4\ \mathrm{cm}) \approx 8$ s, much sorter than the 10 min transfer time demonstrated in Fig. 8.

The rate equation for ^{3}He polarization as a function of postion in the target cell is therefore

$$\frac{dP(r)}{dt} = G_t(P_p - P_t) + D_t \nabla^2 P(r) - P(r)[\Gamma_B(r) + \Gamma_i(r)] \ , \tag{A16}$$

where $\Gamma_B(r)$ is the relaxation rate due to the pulsed beam given by Eqs. (18) and (19) and $\Gamma_i(r)$ is the ionization rate given in Eq. (25).

Wall relaxation is not explicitly written in Eq. (A16); rather, it comes from the boundary conditions imposed by the radial derivative of $P(r)$ at $r=0$ and by the average polarization P_t which is a measured quantity. We assume that $P(r)$ is independent of axial distance along the target cell and azimuthal angle. Thus

$$\nabla^2 P(r) = \frac{1}{r} \frac{\partial}{\partial r} \left[r \frac{\partial P(r)}{\partial r} \right] \ . \tag{A17}$$

The average polarization in the target cell is

$$P_t = \frac{1}{\pi A^2} \int_0^A P(r) 2\pi r \, dr \ . \tag{A18}$$

In the absence of the electron beam [$\Gamma_B(r)=0$ and $\Gamma_i(r)=0$]

$$\frac{dP(r)}{dt} = G_t(P_p - P_t) + D_t \nabla^2 P(r) \ . \tag{A19}$$

In the steady state [$dP(r)/dt=0$] we have

$$\frac{1}{r} \frac{\partial}{\partial r} \left[r \frac{\partial P(r)}{\partial r} \right] = -\frac{G_t}{D_t} (P_p - P_t) \ . \tag{A20}$$

The solutions are

$$\frac{\partial P(r)}{\partial r} = -\frac{r}{2} \frac{G_t}{D_t} (P_p - P_t) \tag{A21}$$

and

$$P(r) = P_t + \frac{G_t}{4D_t} (P_p - P_t) \left[\frac{A^2}{2} - r^2 \right] \ , \tag{A22}$$

which satisfy the boundary conditions $(\partial P/\partial r)|_{r=0}=0$ and Eq. (A18).

In order to establish the connection to Γ_w, the measured relaxation time of the average polarization P_t, we integrate Eq. (A19) radially over the target cell:

$$\frac{1}{A^2} \frac{d}{dt} \int_0^A 2rP(r) dr = \frac{1}{A^2} \int_0^A [G_t(P_p - P_t) + D_t \nabla^2 P(r)] 2r \, dr \ . \tag{A23}$$

The left-hand side yields

$$\frac{dP_t}{dt} = G_t(P_p - P_t) - \Gamma_w P_t \ , \tag{A24}$$

which follows the form of Eq. (A14) and establishes the

definition of Γ_w as the averaged wall relaxation rate. The right-hand side, integrated by parts, yields

$$G_t(P_p-P_t)+2\frac{D_t}{A}\frac{\partial P(r)}{\partial r}\bigg|_{r=A} . \tag{A25}$$

Combining these two equations, we have a boundary condition at $r=A$

$$\frac{\partial P(r)}{\partial r}\bigg|_{r=A}=-\frac{A}{2D_t}\Gamma_w P_t . \tag{A26}$$

Substituting the steady-state solution for $\partial P(A)/\partial r$ we find the expected relation for the steady state:

$$G_t(P_p-P_t)=\Gamma_w P_t , \tag{A27}$$

and Eq. (A22) becomes

$$P(r)=P_t\left[1+\frac{\Gamma_w A^2}{8D_t}\left[1-2\frac{r^2}{A^2}\right]\right] . \tag{A28}$$

For $\Gamma_w=1/(30\text{ h})$, $D_t=1$ cm^2/s and $A=1$ cm, we see that the position dependence is extremely weak:

$$P(r)\approx P_t\left[1+10^{-6}\left[1-2\frac{r^2}{A^2}\right]\right] . \tag{A29}$$

Therefore, $P(r)$ can be accurately expressed as the average over the target cell [$P(r)\approx P_t$] with an effective error less than 1 part in 10^{-6}.

Returning now to Eq. (A16) we investigate the effects of an electron beam on the radial distribution of polarization in the target cell. We recall the radial dependence of relaxation due to the beam:

$$\Gamma_B(r)=\frac{R}{2}\left[\frac{\mu_0 I}{2\pi a B_0}\right]^2\frac{r^2}{a^2}e^{-2r^2/a^2}$$

(pulsed beam) , (A30)

$$\Gamma_B(r)=\frac{DF_D}{2a^2}\left[\frac{\mu_0 I}{2\pi a B_0}\right]^2\left[1-2\frac{r^2}{a^2}\right]^2 e^{-2r^2/a^2}$$

(gradients) , (A31)

$$\Gamma_i(r)=k_{\rm ion}\frac{i_b}{\pi a^2}e^{-r^2/a^2} . \tag{A32}$$

Reiterating the definitions of the quantities: I is the peak current of the electron beam pulses, a is the electron beam radius taken to be 0.05 cm, B_0 is the holding field of about 30 G, R is the beam pulse rate, F_D is the pulsed beam duty factor, $k_{\rm ion}\approx 2.4$ cm^2/C is given by Eq. (27), and i_b is the average of the electron beam. Numerical estimates of the coefficients with parameters for the SLAC beam given in Table I are

$$\frac{R}{2}\left[\frac{\mu_0 I}{2\pi a B_0}\right]^2=1.7\times 10^{-4}\text{ s}^{-1} , \tag{A33}$$

$$\frac{DF_D}{2a^2}\left[\frac{\mu_0 I}{2\pi a B_0}\right]^2=2.2\times 10^{-7}\text{ s}^{-1} \tag{A34}$$

and for $i_b=5$ μA

$$k_{\rm ion}\frac{i_b}{\pi a^2}=1.5\times 10^{-3}\text{ s}^{-1} . \tag{A35}$$

We will therefore specialize our considerations to the distribution of polarization due to ionization, which dominates the beam-induced relaxation as is evident from the average of the relaxation rates given in Table I.

We seek the steady-state solution for the polarization in the target cell with the average beam current i_b. This is appropriate even though the beam is pulsed. In order to see that this is true, we estimate the loss of polarization during a single-beam pulse in the region of the beam. Making use of Eq. (26), the relaxation rate for the Bates beam with peak current $I=1$ mA and $V/t=\pi a^2$ is $\Gamma_{\rm peak}\approx 0.1$ s^{-1}. At Bates, the beam-pulse duration is about 15 μs and thus the polarization loss in the region of the beam during a single beam pulse is $4\times 10^{-6}P_t$. During the time between pulses, about 1.6 ms at Bates, diffusion is driven by the small gradient of polarization effected by the pulse. We use Eq. (A15) to estimate that ^{3}He atoms diffuse about one beam radius during this 1.6 ms, reducing the polarization loss. Successive beam pulses will destroy the polarization, but increase the polarization gradient, leading to a steady-state situation determined by the average of many pulses. It is therefore valid to use the average beam current i_b.

The steady-state distribution of polarization in the target cell is described by the equation

$$\frac{1}{r}\frac{\partial}{\partial r}\left[r\frac{\partial P(r)}{\partial r}\right]=\frac{k_{\rm ion}}{D_t}\frac{i_b}{\pi a^2}e^{-r^2/a^2}P(r)-\frac{\Gamma_t}{D_t}P_t , \tag{A36}$$

where we have used $G_t(P_p-P_t)=\Gamma_t P_t$. The solution can be determined numerically; however, it is instructive to explore the situation by iteration, taking $P(r)=P_t[1+f(r)]$ beginning with $f(r)=0$. Then we find

$$\frac{\partial P(r)}{\partial r}=\frac{k_{\rm ion}}{D_t}\frac{i_b}{2\pi r}[1-e^{-r^2/a^2}]P_t-\frac{\Gamma_t r}{2D_t}P_t . \tag{A37}$$

We use Eq. (A18) and integrate by parts to find

$$P_t=P(A)-\frac{1}{A^2}\int_0^A\frac{\partial P(r)}{\partial r}r^2dr . \tag{A38}$$

Substituting Eq. (A37) into the integral, we have

$$P(A)=P_t\left[1+\frac{k_{\rm ion}i_b}{4D_t}\left[\frac{a^2}{A^2}(e^{-A^2/a^2}-1)+1\right]\right]-\frac{\Gamma_t A^2}{8D_t}P_t \tag{A39}$$

and with $a=0.05$ cm and $A=1$ cm we can write

$$P(A)\approx P_t\left[1+\frac{k_{\rm ion}i_b}{4D_t}-\frac{\Gamma_t A^2}{8D_t}\right] . \tag{A40}$$

This estimated value can be used along with numerical

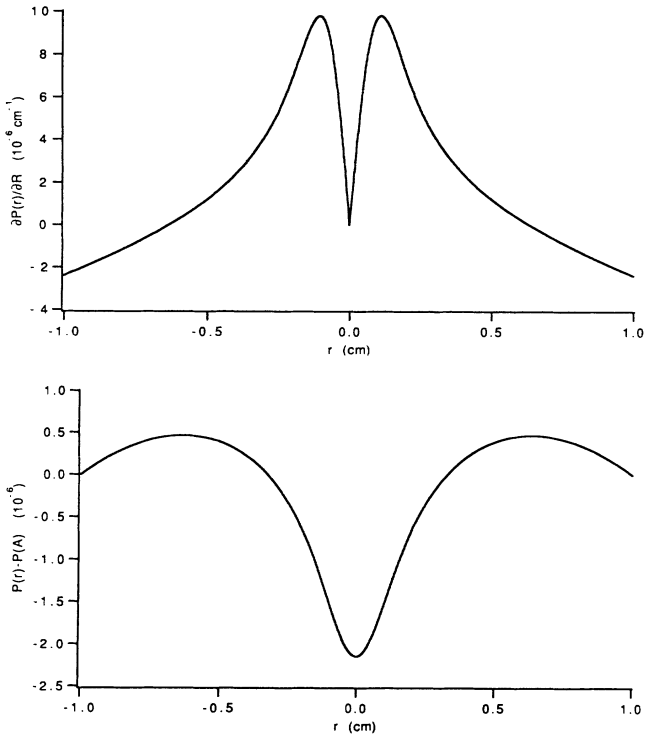

FIG. 11. The calculated radial distribution of target polarization $[P(r)-P(A)]$ and its first derivative for a 10 μA electron beam, and the target parameters used at Bates. For further details, see the description following Eq. (68).

integration of Eq. (A37) to determined a first iteration of $P(r)$. In Fig. 11 we show this first iteration of $\partial P(r)/\partial r$ and $P(r)-P(A)$ for the target configuration used at Bates assuming a 10 μA electron beam, $P_t=40\%$ and a total relaxation rate of $\Gamma_t=1/(15\text{ h})$. The small dip of target polarization (about 2×10^{-6}) near the center of the target is due to the beam, and the drop near the wall is due to wall relaxation. The negligible dependence of target-cell polarization on position justifies our use of the averages P_t and T_t. We therefore write the rate equation for the target cell as

$$\frac{dP_t}{dt}=G_t(P_p-P_t)-\Gamma_t P_t\ , \tag{A41}$$

where

$$\Gamma_t=\Gamma_w+\Gamma_B+\Gamma_i\ . \tag{A42}$$

3. *Target cell rate equations and transfer time calculation*

Equations (A14) and (A41) are a set of coupled equations. The solutions to these coupled differential equations give the time dependence of the ^{3}He polarization in the target cell in terms of the Rb polarization $P_{\rm Rb}$ for the steady-state ($t\rightarrow\infty$) polarization in the target cell. In our current design, the transfer rates G_p and G_t are about $1/(10\text{ min})$, much larger than the rates Γ and $\gamma_{\rm SE}$. Thus we neglect terms of order $\gamma_{\rm SE}\Gamma$ to find

$$P_t(t\rightarrow\infty)=P_p(t\rightarrow\infty)$$
$$=P_{\rm Rb}\frac{n_{\rm Rb}k_{\rm SE}n_pV_p}{n_{\rm Rb}k_{\rm SE}n_pV_p+\Gamma_p n_pV_p+\Gamma_t n_tV_t}\ . \tag{A43}$$

This agrees with the expression given in Eq. (7), which is based on the same assumption that the ^{3}He polarization transfer rates are much greater than spin exchange and relaxation rates.

The expected rate for polarization transfer measured in the tests described in Sec. V is found by combining Eq. (A14) and (A41). Neglecting $\gamma_{\rm SE}$ and Γ relative to G_p and G_t.

$$\frac{d}{dt}(P_p-P_t)=-(G_p+G_t)(P_p-P_t)\ . \tag{A44}$$

The solution for P_p-P_t with initial condition $P_p(0)-P_t(0)$ is

$$P_p(t)-P_t(t)=[P_p(0)-P_t(0)]e^{-(G_p+G_t)t}\ . \tag{A45}$$

Combining this with Eq. (A41) yields

$$\frac{dP_t}{dt}=G_t[P_p(0)-P_t(0)]e^{-(G_p+G_t)t}\ , \tag{A46}$$

which has the solution

$$P_t(t)=\frac{G_t}{G_p+G_t}[P_p(0)-P_t(0)](1-e^{-(G_p+G_t)t})\ . \tag{A47}$$

The rate for polarization transfer is therefore G_p+G_t.

[1] T. E. Chupp, M. E. Wagshul, K. P. Coulter, A. B. McDonald, and W. Happer, Phys. Rev. C **36**, 2224 (1987).
[2] K. P. Coulter, T. E. Chupp, A. B. McDonald, C. D. Bowman, J. D. Bowman, J. J. Szymanski, V. Yuan, G. D. Cates, D. R. Benton, and E. D. Earle, Nucl. Instrum. Methods A **288**, 463 (1990).
[3] A. Rahav *et al.*, Phys. Rev. C (to be published).
[4] B. Larson *et al.*, Phys. Rev. Lett. **67**, 3356 (1991).
[5] N. R. Newbury *et al.*, Phys. Rev. Lett. **67**, 3219 (1991).
[6] B. Blankleider and R. Woloshyn, Phys. Rev. C **29**, 538 (1984).
[7] Proposal to Bates Experimental Program Advisory Committee 88-25, 1988 (unpublished).
[8] R. Woloshyn, Nucl. Phys. **A496**, 749 (1989).
[9] R. Arnold *et al.*, proposal to SLAC Experimental Program Advisory Committee E-142, 1989 (unpublished).
[10] K. P. Coulter, A. B. McDonald, G. D. Cates, W. Happer, and T. E. Chupp, Nucl. Instrum. Methods A **276**, 29 (1989).
[11] T. E. Chupp, R. A. Loveman, M. E. Wagshul, A. M. Bernstein, W. Fong, A. K. Thompson, D. Tieger, K. von-Reden, K. P. Coulter, A. B. McDonald, and W. Happer,

in *High-Energy Spin Physics: Eighth International Symposium, University of Minnesota, 1988,* edited by Kenneth J. Heller, AIP Conference Proceedings No. 187 (AIP, New York, 1989), p. 1320.
[12] M. E. Wagshul and T. E. Chupp, Phys. Rev. A **40**, 4447 (1989).
[13] R. L. Gamblin and T. R. Carver, Phys. Rev. **138**, A946 (1965).
[14] K. P. Coulter, PhD. thesis, Princeton University (1989).
[15] S-Y Che'en and M. Takeo, Rev. Mod. Phys. **29**, 20 (1957).
[16] R. J. Knize, Phys. Rev. A **40**, 6219 (1989).
[17] M. E. Wagshul, PhD. dissertation Harvard University.
[18] D. R. Swenson and L. W. Anderson, Nucl. Instrum. Methods B **29**, 627 (1988).
[19] E. S. Hrycyshyn and L. Krause, Can. J. Phys. **48**, 2761 (1970).
[20] K. Bonin, T. Walker, and W. Happer, Phys. Rev. A **37**, 3270 (1988).
[21] G. D. Cates, S. R. Schaefer, and W. Happer, Phys. Rev. A **37**, 2877 (1988).
[22] R. G. Milner, R. McKeown, and C. Woodward, Nucl. Instrum. Methods A **257**, 286 (1987).
[23] G. Cates, N. Newberry, and A. Barton, private communication.
[24] B. Larson *et al.,* Phys. Rev. A **44**, 3108 (1991).
[25] A. A. Abragham, *Principles of Nuclear Magnetism* (Oxford University Press, London, 1961), p. 34.
[26] D. Beck *et al.,* Phys. Rev. Lett. **59**, 1537 (1987).
[27] T. W. Donnelly and A. S. Raskin, Ann. Phys. (N.Y.) **169**, 247 (1986).
[28] A. K. Thompson *et al.* Harvard report, 1991.

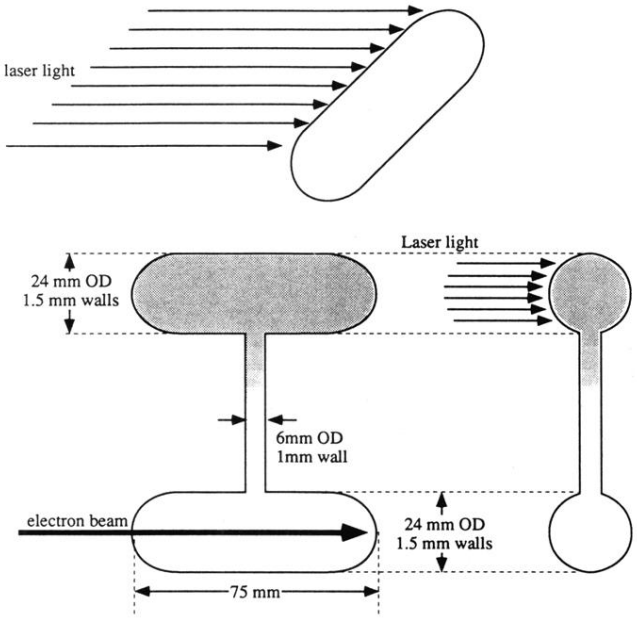

FIG. 1. A schematic illustration of the two-cell target. The upper cell is the pumping volume (V_p) and the lower cell is the target volume (V_t). The Rb is confined to the upper cell by a thermal gradient along the transfer tube.

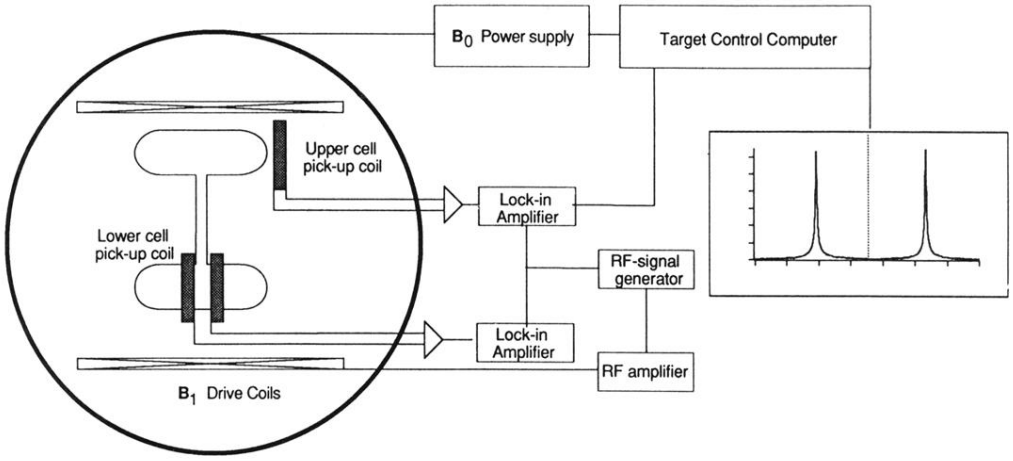

FIG. 4. Schematic of the NMR ^{3}He polarimeter. Pickup coils can monitor the polarization in both the pumping cell and target cell, though during electron bombardment, only the pumping cell polarization is monitored. The control computer sweeps the $\mathbf{B}_0$ field through the resonance of the ^{3}He with the applied rf $\mathbf{B}_1$ field. The magnetization precessing about $\mathbf{B}_0$ at the Larmor frequency induces a voltage in the pickup coil which is detected by the lock-in amplifiers. The computer records the NMR signal vs $\mathbf{B}_0$.